







Emergence of subharmonics in a microwave driven dissipative Rydberg gas

Zong-Kai Liu ^{1,2,*},† Kong-Hao Sun ^{1,2,*}, Albert Cabot ³, Federico Carollo ³, Jun Zhang,^{1,2} Zheng-Yuan Zhang,^{1,2} Li-Hua Zhang,^{1,2} Bang Liu,^{1,2} Tian-Yu Han,^{1,2} Qing Li,^{1,2} Yu Ma,^{1,2} Han-Chao Chen,^{1,2} Igor Lesanovsky ^{3,4}, Dong-Sheng Ding ^{1,2,‡} and Bao-Sen Shi^{1,2}

¹Key Laboratory of Quantum Information, *University of Science and Technology of China, Hefei, Anhui 230026, China*

²Synergetic Innovation Center of Quantum Information and Quantum Physics, *University of Science and Technology of China, Hefei, Anhui 230026, China*

³Institut für Theoretische Physik, *Eberhard Karls Universität Tübingen, Auf der Morgenstelle 14, 72076 Tübingen, Germany*

⁴School of Physics and Astronomy and Centre for the Mathematics and Theoretical Physics of Quantum Non-Equilibrium Systems, *The University of Nottingham, Nottingham, NG7 2RD, United Kingdom*



(Received 11 February 2024; accepted 15 August 2024; published 18 September 2024)

Quantum many-body systems near phase transitions respond collectively to externally applied perturbations. We explore this phenomenon in a laser-driven dissipative Rydberg gas that is tuned to a bistable regime. Here two metastable phases coexist, which feature a low and high density of Rydberg atoms, respectively. The ensuing collective dynamics, which we monitor *in situ*, is characterized by stochastic collective jumps between these two macroscopically distinct many-body phases. We show that the statistics of these jumps can be controlled using a dual-tone microwave field. In particular, we find that the distribution of jump times develops peaks corresponding to subharmonics of the relative microwave detuning. Our study demonstrates the control of collective statistical properties of dissipative quantum many-body systems without the necessity of fine-tuning or of ultracold temperatures. Such robust many-body phenomena may find technological applications in sensing.

DOI: [10.1103/PhysRevResearch.6.L032069](https://doi.org/10.1103/PhysRevResearch.6.L032069)

Open many-body quantum systems in which dissipative processes and coherent interactions compete may display emergent behavior. This manifests in novel timescales and dynamical regimes, which are not simply predictable from the knowledge of the underlying microscopic physics alone. For example, symmetries of the microscopic equations of motion can be spontaneously broken and as a consequence nonergodic dynamical behavior occurs. Further to that, the entire system responds collectively to externally applied perturbations. Not only can such a mechanism be exploited in practical applications, such as collectively enhanced sensing devices [1–3], but it may also underlie the physics of learning, as demonstrated in the case of pattern retrieval dynamics in the Hopfield neural network model [4].

In recent years Rydberg gases have become a widely employed system for the investigation of many-body physics. The Rydberg platform features strong long-range interactions [5–7] together with dissipation channels, which enabled the study of nonequilibrium phase transitions [8–14] and the observation of signatures of self-organization [15–18], as well as

of ergodicity breaking and synchronization [19–22]. Besides, Rydberg gases are systems where bistabilities can be created in a robust way without the requirement of cold temperatures or the need of any fine-tuning. Moreover, by choosing suitable Rydberg states it is possible to select the frequency range of the perturbation to which the response of the gas is most dramatic.

Here we demonstrate an experiment conducted in the metastable (or bistable) [8,11,23,24] regime of a dissipative Rydberg gas, where two phases—one with low and one with high Rydberg density—coexist. Dynamically this coexistence manifests in the random switching of the Rydberg density, with exponentially distributed switching times. We monitor this macroscopic effect continuously and nondestructively via an electromagnetically induced transparency (EIT) detection method. We show that by applying a periodic external perturbation, via a dual-tone microwave (MW) electric field, the collective dynamical behavior of the Rydberg gas can be dramatically altered. This manifests directly in the statistics of the switching times, which ceases to be continuous and develops instead discrete peaks at multiples of the period associated with the relative detuning of the MW drive.

Before going to the detailed description of our experimental findings, we illustrate the central idea of our work in Fig. 1. In our setup we excite Rydberg states from hot atomic vapor, where the atomic density is sufficiently large such that atoms in Rydberg states strongly interact. As shown in a number of previous works [24–27], this induces nonlinear and bistable behavior. The latter manifests for instance in a sudden jump from low density ρ_{low} to high density ρ_{high} of Rydberg atoms,

*These authors contributed equally to this work.

†Present address: Shanxi University.

‡Contact author: dds@ustc.edu.cn

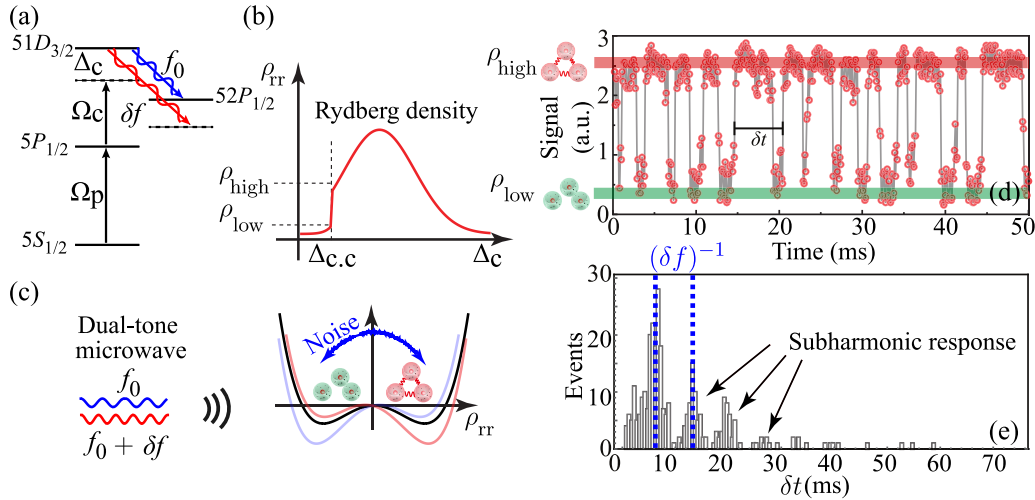


FIG. 1. Collective quantum jumps. (a) Schematic diagram of experimental energy levels. Ω_p and Ω_c are the Rabi frequency of probe and coupling light, respectively, and Δ_c is detuning of coupling light. The blue (upper) arrow represents the microwave field at resonance, while the red (lower) arrow represents the microwave field with a detuning of δf . (b) Sketch of the stationary density in an ensemble of laser-driven Rydberg atoms as a function of the detuning Δ of the Rydberg excitation laser. A sudden change between two phases (ρ_{low} and ρ_{high}) occurs at a detuning $\Delta_{c,c}$. (c) The central features of the physics in this bistable regime are effectively captured by a double-well model. Driving the Rydberg manifold via dual-tone MW fields, with frequencies f_0 and $f_0 + \delta f$, periodically modulates the potential landscape (see different curves). (d) Collective jumps between the two phases appear in the time-resolved transmission signal, here in the presence of the MW field (a.u. stands for arbitrary units, as the transmission signal is obtained through the voltage of the detector). (e) Histogram of the time intervals δt between consecutive upwards jumps (from low to high Rydberg density) for the data in panel (d). Here, the histogram develops characteristic peaks corresponding to subharmonics of the frequency difference δf between the dual-tone MW field components.

ρ_{rr} , when one of the system parameters is tuned. Figures 1(a) and 1(b) are sketches for a situation in which the detuning Δ of the excitation laser is varied. This sudden change can be interpreted [11] by evoking an analogy with equilibrium thermodynamics: one may assume that the stationary state in the bistable regime is governed by an effective potential, which exhibits a double-well shape, as sketched in Fig. 1(c). The two minima correspond to two phases. Close to the transition point, i.e., near $\Delta_{c,c}$ shown in Fig. 1(b), the system performs collective jumps, switching between the two phases with macroscopically distinct Rydberg densities [see transmission signal in Fig. 1(d) which shows data obtained using our EIT detection method]. This qualitative picture can be put on a solid theoretical footing using the theory of metastability [28,29] and in the Supplemental Material [30] we provide more details on this aspect. The switching is stochastic, i.e., it is driven by noise, and the characteristic time δt between consecutive jumps from the low-density towards the high-density phase follows an exponential distribution (see Supplemental Material [30]). As shown in Fig. 1(e), the application of a dual-tone MW field, with relative frequency difference δf [see Fig. 1(a)] leads to a noncontinuous distribution for the times δt . In particular, the resulting distribution exhibits peaks at times that are multiples of $1/\delta f$.

Experimental setup. In our experiment rubidium-85 atoms are placed into a 10 cm long heated glass cell and the temperature is stabilized to 45.0 °C (atomic density $9.19 \times 10^{10} \text{ cm}^{-3}$). Atoms are excited from the ground state ($5S_{1/2}$, $F = 2$) to the Rydberg state ($51D_{3/2}$) via a two-photon process. A 795 nm probe light (with $1/e^2$ -waist radius of approximately 500 μm and peak value of Rabi frequency

$\Omega_p/2\pi \sim 10 \text{ MHz}$) excites atoms from the ground state to the intermediate level ($5P_{1/2}$, $F = 3$) and a further coupling laser with wavelength 480 nm (with $1/e^2$ -waist radius of approximately 200 μm and peak value of Rabi frequency $\Omega_c/2\pi \sim 10 \text{ MHz}$) takes atoms to the Rydberg state. This is an EIT configuration, where the coupling light controls the absorption of the probe light. To observe the EIT spectrum, the detuning of the coupling light Δ_c is scanned while the probe light detuning Δ_p is resonant to the transition $5S_{1/2} - 5P_{1/2}$. The Rabi frequency of the probe light and its detuning are both fixed. After setting the detuning of the coupling light to a specific value Δ_c , the time evolution of the transmission signal is obtained, yielding curves such as the one depicted in Fig. 2(a). In this way, we can study the collective response of the Rydberg gas through the time-dependent transmission.

Besides the probe and coupling beams, there is a dual-tone MW field applied to Rydberg atoms by a MW generator and a horn close to the rubidium glass cell. The polarization of the MW field is linear and one MW field is resonant with the Rydberg transition $51D_{3/2} - 52P_{1/2}$. Here, $51D_{3/2}$ is the Rydberg state in EIT configuration. The lifetimes of the atoms (including spontaneous emission and blackbody radiation at a temperature of 45.0 °C) in these energy levels are $7.13 \times 10^{-2} \text{ ms}$ (for $51D_{3/2}$) and $9.48 \times 10^{-3} \text{ ms}$ (for $52P_{1/2}$), respectively [31]. A second MW field is detuned from this resonance by an amount δf . Specifically, this dual-tone MW field has the form $E_{MW1} \sin(2\pi f_0 t) + E_{MW2} \sin(2\pi [f_0 + \delta f] t)$, where $f_0 = 16.67 \text{ GHz}$ is near resonant with the $51D_{3/2} - 52P_{1/2}$ transition and $\delta f = 300 \text{ Hz}$ represents the relative MW field detuning. The amplitude of the first MW field is fixed at $E_{MW1} = 3.8 \text{ mV/cm}$ and that of the second MW field can

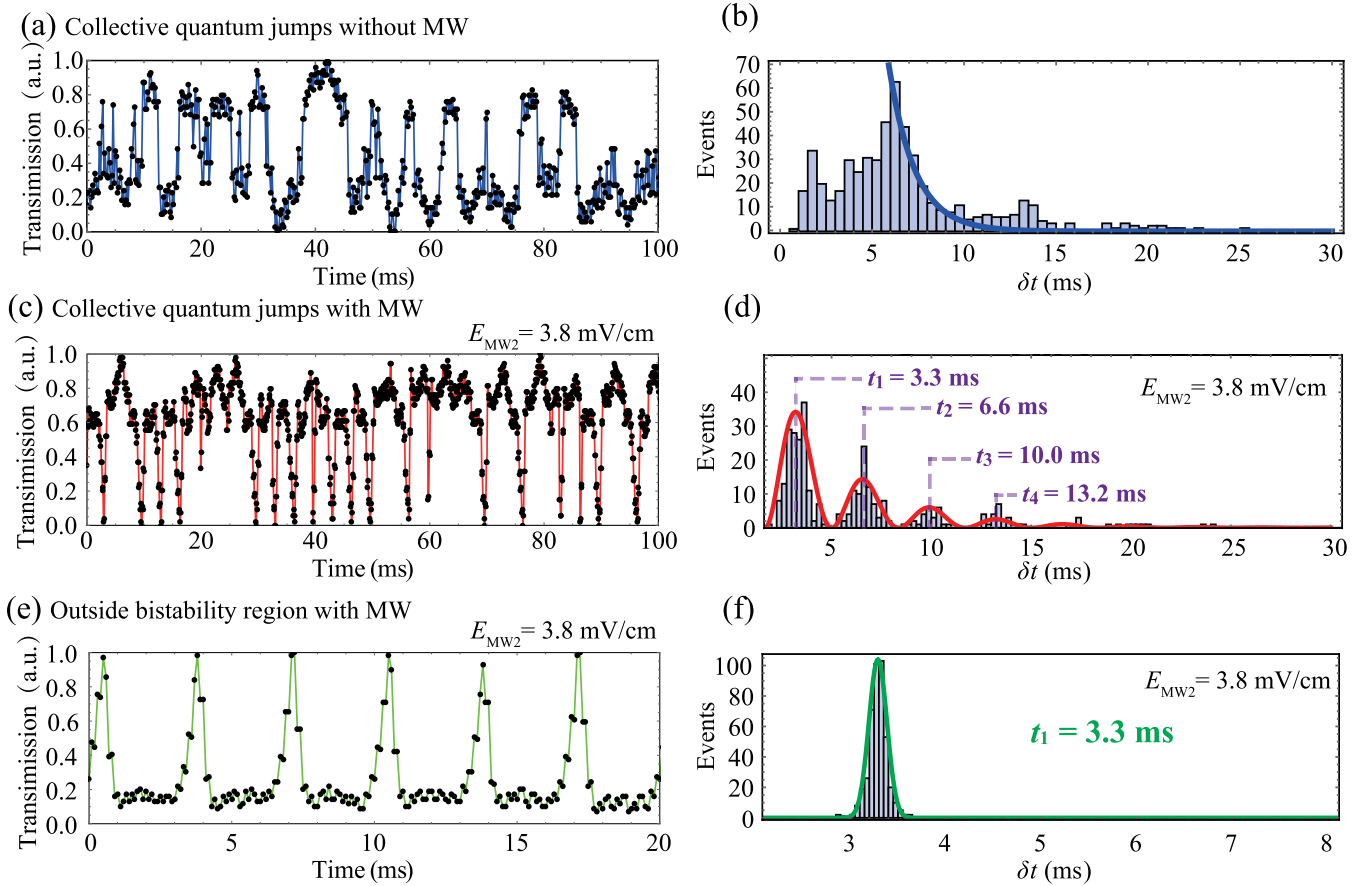


FIG. 2. Controlling the collective quantum jump statistics. (a) Transmission signal showing collective jumps in the absence of MW driving in the bistable region. (b) The corresponding histogram of the time interval δt between consecutive upwards jumps from low to high density [see Fig. 1(b)] displays exponential behavior, given by the fit $g_1(\delta t) \propto \exp(-0.7 \delta t/\text{ms})$ (solid line). (c) Transmission signal in the presence of MW driving. The Rabi frequency of the probe light is $\Omega_p/2\pi = 7$ MHz, which is the same as that in the (a) panel. (d) The histogram for the case in (c) displays peaks occurring at multiples of the modulation period (see labels). The solid line corresponds to the fit $g_2(\delta t) \propto \exp(-0.26 \delta t/\text{ms})[\sin(1.88 \delta t/\text{ms} + \pi/2) + 1]$. (e) Transmission signal far from the bistable regime and in the presence of MW driving. The Rabi frequency of the probe light is $\Omega_p/2\pi = 1$ MHz. (f) Histogram of the time intervals between peaks in (e). The solid line corresponds to the fit $g_3(\delta t) \propto \exp(-56[\delta t/\text{ms} - 3.3]^2)$. All data are obtained for the same detuning Δ_c and Δ_p . In panels (a),(b) there is no MW. In panels (c)–(f) the dual-tone MW field of amplitude $E_{\text{MW}2} = 3.8$ mV/cm is applied. In panels (e), (f) the Rabi frequency of the probe light is lower than that in panels (a)–(d), such that there is no bistable effect.

be attenuated during the experiment. The effective Rabi frequency of the dual-tone MW field is then modulated according to $\Omega_{\text{MW}}(t) = \Omega_{\text{MW}1} + \Omega_{\text{MW}2} \exp(-i2\pi \delta f t)$, where $\Omega_{\text{MW}1(2)}$ corresponds to the Rabi frequency of the MW field resonant (detuned by δf) to the Rydberg states. The MW frequency resonant to the transition $51D_{3/2} - 52P_{1/2}$ ($f_0 = 16.67$ GHz) is calculated via the method reported in Ref. [31]. The amplitude of the MW in the center of the rubidium cell is calibrated by peak splitting of the EIT spectrum according to the Autler-Townes split [32] (for more details see Supplemental Material [30]).

Statistics of collective quantum jumps. As discussed previously and sketched in Fig. 1, stochastic collective jumps manifest in the transmission signal. To establish a benchmark, we show this phenomenon in Fig. 2(a) in the absence of the MW field. We choose Rabi frequency and detuning of the probe and coupling light such that the system is located in a bistable parameter region. The physical process underlying the collective jumps was discussed in Ref. [8]. The jump

process from the low ρ_{low} to the high density phase ρ_{high} (upward jump) is analogous to the collective jump in the double-well model, where the fluctuation [noise in Fig. 1(c)] in the Rydberg population triggers an avalanche or facilitation of Rydberg excitations. As argued in Ref. [8] also the downward jump (from high to low density) is collective.

On a more formal level, the intermittent dynamics originating from the collective jumps can be understood from the theory of metastability [28,29]. Here the low- and the high-density phase correspond to two metastable states that are approximate steady states of the dynamical generator that governs the time evolution of the dissipative Rydberg gas. These two states are connected via an effective classical stochastic dynamics that entails collective jumps between them. This predicts that the time interval δt between two consecutive upwards jumps follows an exponential distribution for sufficiently large δt (see Supplemental Material [30]). As shown in Figs. 2(a) and 2(b) this is indeed confirmed by our experiment. To produce histograms as shown

in Fig. 2(b), we collect 20 sets of transmission signals with same length 100 ms, one of which is shown in Fig. 2(a), and count how often a time interval of length δt occurs between two consecutive upward jumps (from the low- to the high-density phase). The details of the procedure for generating the histograms from the transmission signals are given in the Supplemental Material [30]. Note that, at small δt , there is a hole in the histogram. This is a consequence of “antibunching” in two-level systems: after an upward jump, a downward jump has to occur first, before the next upward jump can take place. This limits the smallest value of δt that is observable.

In the second and third row of Fig. 2 we show data obtained in the presence of the dual-tone MW field. We distinguish here the case in which the system is initially in the bistable region [Figs. 2(c) and 2(d)] from the case in which the system is initially far from it [Figs. 2(e) and 2(f)]. For a bistable system the application of the MW leads to a drastic change of the distribution of the jump times, as shown in Fig. 2(d). The histogram breaks up into multiple disconnected peaks with an exponentially decaying envelope. This is indeed a collective response to the dual-tone MW, which can be seen by making a comparison with the case in which the system is far from a bistable regime. Here, the application of the MW with oscillating Rabi frequency Ω_{MW} merely modulates the transmission signal monochromatically; see Fig. 2(e). The associated histogram, shown in Fig. 2(f), displays a single peak at $\delta t = t_1 \approx 3.3$ ms, which corresponds to the relative detuning of the dual-tone MW field: $\delta f = 300$ Hz. The bistable system, however, responds not only at that frequency, but also features collective subharmonic responses: a second, a third, and a fourth peak appear in Fig. 2(d), labeled as $t_2 = 6.6$ ms, $t_3 = 10.0$ ms, and $t_4 = 13.2$ ms.

Tunable response. To characterize the observed subharmonic response, we vary the amplitude of the second MW field E_{MW2} , as quantified by the parameter $\beta = 20 \log_{10}(E_{MW2}/E_{MW1})$, and the frequency difference δf . As shown in Fig. 3(a), upon decreasing E_{MW2} the subharmonic peaks decrease in height and broaden, while remaining in their position. As apparent in the bottom panel of Fig. 3(a), the distribution approaches a continuous one for sufficiently weak driving E_{MW2} . To understand the origin of the subharmonic response, we consider a simple mean-field model described by a Lindblad master equation [2]. At the mean-field level, the presence of many-body interactions between Rydberg atoms results in a nonlinear shift of the detuning which depends on the Rydberg state density. In addition, we include a noise term in the detuning, encoding thermal fluctuations (see Supplemental Material [30]). The latter term is crucial for the emergence of the subharmonic response (for details on the theoretical model see Supplemental Material [30]). The distribution of δt calculated with our model is illustrated in Fig. 3(b), as a function of the amplitude of the second MW field, E_{MW2} . It is important to note that the theoretical model employed in our study is primarily designed to capture qualitative features of the observed phenomenology rather than providing precise quantitative predictions. Several experimental factors, such as laser noise and atomic velocity distribution, were not considered in our model.

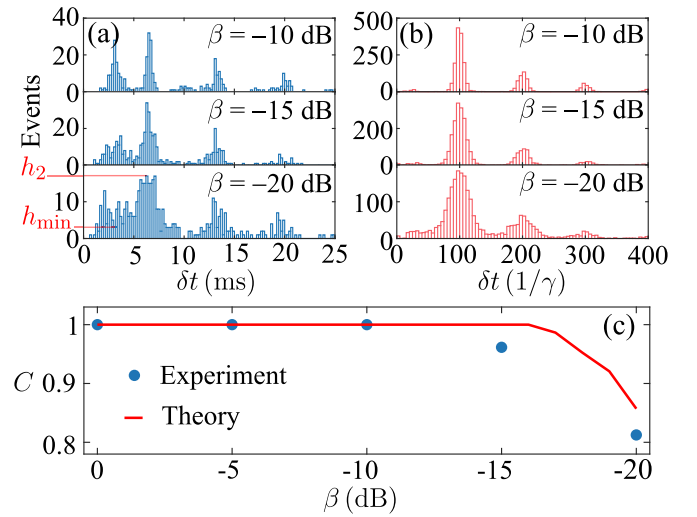


FIG. 3. Jump time distributions as a function of MW intensity. (a) Experimentally measured distributions of δt for different values of β , from -10 dB to -20 dB, and $\delta f = 300$ Hz. (b) Distributions of δt obtained with our theoretical model for values of β as in (a) and $\delta f = 0.01\gamma$. Here γ is the lifetime of the Rydberg state in our theoretical model. Details are given in the Supplemental Material [30]. (c) Behavior of the contrast $C = (h_2 - h_{\min})/h_2$ as a function of the parameter β . Here, h_2 is the height of the second peak and h_{\min} is the minimum height of the bins between the first and the second peak [see bottom of panel (a) for an example]. We display results from both experimental (bullet) and theoretical (solid line) data.

The change of the jump time distribution upon decreasing the driving intensity E_{MW2} can be understood in terms of the double-well model discussed at the beginning [please see Fig. 1(c) and Supplemental Material [30] for further details on the double-well potential and its underlying physics]. The driving modulates the “potential landscape” periodically in a way that gives rise to an optimal time within the period, at which collective jumps are favored. When the modulation is strong in comparison to the noise this leads to narrow peaks in the distribution [cf. Fig. 2(c)]. However, as the driving weakens, the modulation of the potential is less effective and noise becomes the main driver for the collective jumps. In this case, there is no preferred time for their occurrence and the distribution broadens.

To characterize the broadening of the peaks, we define the quantity $C = (h_2 - h_{\min})/h_2$, which measures the contrast between the height of the second peak, h_2 , and the minimum height of the bins between the first and the second peak, h_{\min} . As illustrated in Fig. 3(c), when the amplitude of the second MW field is decreased below a threshold value, the contrast becomes smaller than one, indicating the merging of the first and the second peak. This behavior is also captured by our theoretical model.

In Fig. 4, we present data showing how the distribution of δt changes with the MW frequency difference δf , in both (a)–(c) experiment and (d)–(f) theoretical model. This illustrates that the subharmonic response persists for varying δf . Furthermore, as the value of δf increases, the detuned MW field gradually decouples from the system and only the resonant MW field is relevant. Consequently, the distribution of

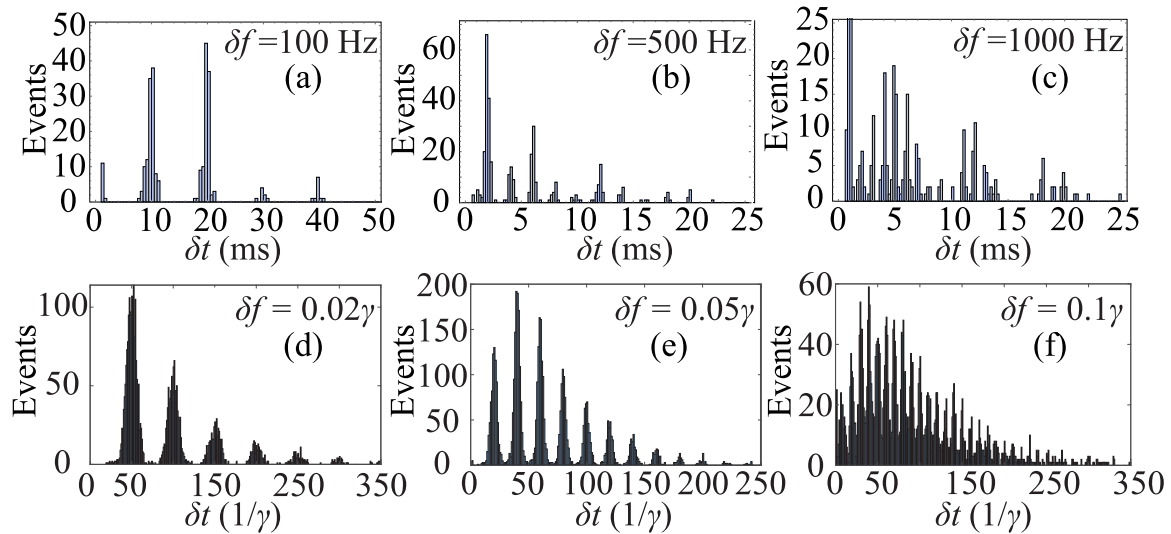


FIG. 4. Experimental and theoretical distribution of the collective quantum jump times as a function of the MW frequency difference δf . (a)–(c) Experimental distribution of the jump times for different relative detunings of the double-tune MW, $\delta f = 100$ Hz (a), 500 Hz (b), and 1000 Hz (c). The distance between neighboring peaks changes with δf . (d)–(f) Distribution of the jump times calculated through our theoretical model.

δt changes from a subharmonic distribution to an exponential distribution.

Discussion. We have demonstrated that driving a bistable Rydberg-atom system, via a dual-tone MW field, can change the distribution of the times between collective jumps. The latter passes from a late time exponential distribution to one with several peaks corresponding to subharmonics of the relative MW detuning. Details of the distribution can be controlled by varying the amplitude and the detuning of the dual-tone MW fields.

The relevance of the observed phenomenon is not restricted to Rydberg gases. Related features are observed in other settings, such as non-Hermitian systems as well as in dynamical models studied in neuroscience, psychology, and biology [33–38]. In the presence of a periodic driving in these bistable systems, internal or external fluctuations can trigger phenomena similar to the one described here. Our work sheds light on how collective nonlinear macroscopic behavior is linked to the microscopic behavior of the many-body system. Establishing such a connection is notoriously difficult, especially in quantum systems. Further, the observed collective effects may lead to increase of the signal-to-noise ratio during sensing in a noisy environment through the so-called stochastic resonance effect [39–42].

Acknowledgments. D.-S.D acknowledges discussions with Prof. J. Ye from JILA and appreciates instructive comments from Dr. D. Malz, Prof. C. S. Adams, and Prof. W. Yi. We acknowledge funding from the National Key R&D Program of China (Grant No. 2022YFA1404002), the National Natural Science Foundation of China (Grants No. U20A20218, No. 61525504, No. 61435011, and No. 123B2062), the Anhui Initiative in Quantum Information Technologies (Grant No. AHY020200), and the major science and technology projects in Anhui Province (Grant No. 202203a13010001). A.C. and I.L. acknowledge funding from the Deutsche Forschungsgemeinschaft (DFG, German Research Foundation) through the Research Units FOR 5413/1, Grant No. 465199066, and the Walter Benjamin programme, Grant No. 519847240. I.L. also received funding from the European Union’s Horizon Europe research and innovation program under Grant Agreement No. 101046968 (BRISQ) and gratefully acknowledges support within the QuantERA II Programme that has received funding from the EU’s H2020 research and innovation programme under the Grant Agreement No. 101017733. F.C. is indebted to the Baden-Württemberg Stiftung for the financial support of this research project by the Eliteprogramme for Postdocs.

-
- [1] J. S. Aldridge and A. N. Cleland, Noise-enabled precision measurements of a duffing nanomechanical resonator, *Phys. Rev. Lett.* **94**, 156403 (2005).
- [2] C. G. Wade, M. Marcuzzi, E. Levi, J. M. Kondo, I. Lesanovsky, C. S. Adams, and K. J. Weatherill, A terahertz-driven non-equilibrium phase transition in a room temperature atomic vapour, *Nat. Commun.* **9**, 3567 (2018).
- [3] M. Raghunandan, J. Wrachtrup, and H. Weimer, High-density quantum sensing with dissipative first order transitions, *Phys. Rev. Lett.* **120**, 150501 (2018).
- [4] J. J. Hopfield, Neural networks and physical systems with emergent collective computational abilities, *Proc. Natl. Acad. Sci. USA* **79**, 2554 (1982).
- [5] M. Saffman, T. G. Walker, and K. Mølmer, Quantum information with Rydberg atoms, *Rev. Mod. Phys.* **82**, 2313 (2010).
- [6] C. S. Adams, J. D. Pritchard, and J. P. Shaffer, Rydberg atom quantum technologies, *J. Phys. B: At., Mol., Opt. Phys.* **53**, 012002 (2019).
- [7] A. Browaeys and T. Lahaye, Many-body physics with individually controlled Rydberg atoms, *Nat. Phys.* **16**, 132 (2020).

- [8] T. E. Lee, H. Häffner, and M. C. Cross, Collective quantum jumps of Rydberg atoms, *Phys. Rev. Lett.* **108**, 023602 (2012).
- [9] C. Carr, R. Ritter, C. G. Wade, C. S. Adams, and K. J. Weatherill, Nonequilibrium phase transition in a dilute Rydberg ensemble, *Phys. Rev. Lett.* **111**, 113901 (2013).
- [10] H. Schempp, G. Günter, M. Robert-de Saint-Vincent, C. S. Hofmann, D. Breyel, A. Komnik, D. W. Schönleber, M. Gärtner, J. Evers, S. Whitlock, and M. Weidemüller, Full counting statistics of laser excited rydberg aggregates in a one-dimensional geometry, *Phys. Rev. Lett.* **112**, 013002 (2014).
- [11] M. Marcuzzi, E. Levi, S. Diehl, J. P. Garrahan, and I. Lesanovsky, Universal nonequilibrium properties of dissipative Rydberg gases, *Phys. Rev. Lett.* **113**, 210401 (2014).
- [12] I. Lesanovsky and J. P. Garrahan, Out-of-equilibrium structures in strongly interacting Rydberg gases with dissipation, *Phys. Rev. A* **90**, 011603(R) (2014).
- [13] A. Urvoy, F. Ripka, I. Lesanovsky, D. Booth, J. P. Shaffer, T. Pfau, and R. Löw, Strongly correlated growth of Rydberg aggregates in a vapor cell, *Phys. Rev. Lett.* **114**, 203002 (2015).
- [14] D.-S. Ding, Z.-K. Liu, B.-S. Shi, G.-C. Guo, K. Mølmer, and C. S. Adams, Enhanced metrology at the critical point of a many-body Rydberg atomic system, *Nat. Phys.* **18**, 1447 (2022).
- [15] D.-S. Ding, H. Busche, B.-S. Shi, G.-C. Guo, and C. S. Adams, Phase diagram of non-equilibrium phase transition in a strongly-interacting Rydberg atom vapour, *Phys. Rev. X* **10**, 021023 (2020).
- [16] S. Helmrich, A. Arias, G. Lochead, T. M. Wintermantel, M. Buchhold, S. Diehl, and S. Whitlock, Signatures of self-organized criticality in an ultracold atomic gas, *Nature (London)* **577**, 481 (2020).
- [17] T. M. Wintermantel, Y. Wang, G. Lochead, S. Shevate, G. K. Brennen, and S. Whitlock, Unitary and nonunitary quantum cellular automata with Rydberg arrays, *Phys. Rev. Lett.* **124**, 070503 (2020).
- [18] K. Klocke, T. M. Wintermantel, G. Lochead, S. Whitlock, and M. Buchhold, Hydrodynamic stabilization of self-organized criticality in a driven Rydberg gas, *Phys. Rev. Lett.* **126**, 123401 (2021).
- [19] F. M. Gambetta, F. Carollo, M. Marcuzzi, J. P. Garrahan, and I. Lesanovsky, Discrete time crystals in the absence of manifest symmetries or disorder in open quantum systems, *Phys. Rev. Lett.* **122**, 015701 (2019).
- [20] K. Wadenpfehl and C. S. Adams, Emergence of synchronization in a driven-dissipative hot Rydberg vapor, *Phys. Rev. Lett.* **131**, 143002 (2023).
- [21] D. Ding, Z. Bai, Z. Liu, B. Shi, G. Guo, W. Li, and C. S. Adams, Ergodicity breaking from Rydberg clusters in a driven-dissipative many-body system, *Sci. Adv.* **10**, eadi5893 (2024).
- [22] X. Wu, Z. Wang, R. G. Fan Yang, C. Liang, M. K. Tey, X. Li, T. Pohl, and L. You, Observation of a dissipative time crystal in a strongly interacting Rydberg gas, *Nat. Phys.* (2024), doi:10.1038/s41567-024-02542-9.
- [23] C. G. Wade, N. Šibalić, N. R. de Melo, J. M. Kondo, C. S. Adams, and K. J. Weatherill, Real-time near-field terahertz imaging with atomic optical fluorescence, *Nat. Photon.* **11**, 40 (2017).
- [24] F. Letscher, O. Thomas, T. Niederprüm, M. Fleischhauer, and H. Ott, Bistability versus metastability in driven dissipative Rydberg gases, *Phys. Rev. X* **7**, 021020 (2017).
- [25] D. Weller, A. Urvoy, A. Rico, R. Löw, and H. Kübler, Charge-induced optical bistability in thermal Rydberg vapor, *Phys. Rev. A* **94**, 063820 (2016).
- [26] N. R. de Melo, C. G. Wade, N. Šibalić, J. M. Kondo, C. S. Adams, and K. J. Weatherill, Intrinsic optical bistability in a strongly driven Rydberg ensemble, *Phys. Rev. A* **93**, 063863 (2016).
- [27] D. Weller, J. P. Shaffer, T. Pfau, R. Löw, and H. Kübler, Interplay between thermal Rydberg gases and plasmas, *Phys. Rev. A* **99**, 043418 (2019).
- [28] K. Macieszczak, M. Guță, I. Lesanovsky, and J. P. Garrahan, Towards a theory of metastability in open quantum dynamics, *Phys. Rev. Lett.* **116**, 240404 (2016).
- [29] K. Macieszczak, D. C. Rose, I. Lesanovsky, and J. P. Garrahan, Theory of classical metastability in open quantum systems, *Phys. Rev. Res.* **3**, 033047 (2021).
- [30] See Supplemental Material at <http://link.aps.org/supplemental/10.1103/PhysRevResearch.6.L032069> for details about generation and calibration of microwave, method for counting the interval of collective jumps, the role of noise and theoretical models.
- [31] N. Šibalić, J. D. Pritchard, C. S. Adams, and K. J. Weatherill, ARC: An open-source library for calculating properties of alkali Rydberg atoms, *Comput. Phys. Commun.* **220**, 319 (2017).
- [32] J. A. Sedlacek, A. Schwettmann, H. Kübler, R. Löw, T. Pfau, and J. P. Shaffer, Microwave electrometry with Rydberg atoms in a vapour cell using bright atomic resonances, *Nat. Phys.* **8**, 819 (2012).
- [33] J. E. Rose, J. F. Brugge, D. J. Anderson, and J. E. Hind, Phase-locked response to low-frequency tones in single auditory nerve fibers of the squirrel monkey, *J. Neurophysiol.* **30**, 769 (1967).
- [34] A. Longtin, A. Bulsara, D. Pierson, and F. Moss, Bistability and the dynamics of periodically forced sensory neurons, *Biol. Cybern.* **70**, 569 (1994).
- [35] L. Gammitoni, P. Hänggi, P. Jung, and F. Marchesoni, Stochastic resonance, *Rev. Mod. Phys.* **70**, 223 (1998).
- [36] A. Calim, T. Palabas, and M. Uzuntarla, Stochastic and vibrational resonance in complex networks of neurons, *Philos. Trans. R. Soc. A* **379**, 20200236 (2021).
- [37] Z. Li, C. Li, G. Xu, W. Chen, Z. Xiong, H. Jing, J. S. Ho, and C.-W. Qiu, Synergetic positivity of loss and noise in nonlinear non-Hermitian resonators, *Sci. Adv.* **9**, eadi0562 (2023).
- [38] A. Schilling, W. Sedley, R. Gerum, C. Metzner, K. Tziridis, A. Maier, H. Schulze, F.-G. Zeng, K. J. Friston, and P. Krauss, Predictive coding and stochastic resonance as fundamental principles of auditory phantom perception, *Brain* **146**, 4809 (2023).
- [39] A. Dodda, A. Oberoi, A. Sebastian, T. H. Choudhury, J. M. Redwing, and S. Das, Stochastic resonance in MoS₂ photodetector, *Nat. Commun.* **11**, 4406 (2020).
- [40] F. Li, F. Duan, F. Chapeau-Blondeau, and D. Abbott, Signal estimation and filtering from quantized observations via adaptive stochastic resonance, *Phys. Rev. E* **103**, 052108 (2021).
- [41] Z. Li, C. Li, Z. Xiong, G. Xu, Y. R. Wang, X. Tian, X. Yang, Z. Liu, Q. Zeng, R. Lin, Y. Li, J. K. W. Lee, J. S. Ho, and C.-W. Qiu, Stochastic exceptional points for noise-assisted sensing, *Phys. Rev. Lett.* **130**, 227201 (2023).
- [42] K.-D. Wu, C. Xie, C.-F. Li, G.-C. Guo, C.-L. Zou, and G.-Y. Xiang, Nonlinearity-enhanced continuous microwave detection based on stochastic resonance, [arXiv:2402.00273](https://arxiv.org/abs/2402.00273).